Biologically-inspired wideband target localisation

Reich, Galen; Antoniou, Michail; Baker, Chris

DOI:
10.1049/iet-rsn.2018.5302

IET Research Journals

Radar, Sonar & Navigation Special Section: Cognitive Radar

IET Journals
The Institution of Engineering and Technology

ISSN 1751-8784
doi: 0000000000
www.ietdl.org

Biologically-inspired wideband target localisation

Galen M. Reich[1] *Michail Antoniou*[1*] *Christopher J. Baker*[1]

[1] *Department of Electronic, Electrical and Systems Engineering, University of Birmingham , United Kingdom*
[*] *E-mail: m.antoniou@bham.ac.uk*

Abstract: In this paper we present two biologically-inspired angular localisation techniques for radar which separately use the magnitudes and phases of the wideband received signals as the cues for angular target localisation. By comparison with predetermined map functions, the angle to a target may be estimated with good accuracy and over a wide angular range of operation. These techniques are implemented in a radar system with a single transmitter and two offset receiving antennas, allowing us to draw upon cues derived from biological systems that are often only explored in psychology, biology, and psychoacoustics.

1 Introduction

The natural world contains a great many echolocating species: animals that expertly use acoustic calls to enhance perception of their environment. Radar systems are based on the principles of echolocation, and use electromagnetic radiation to build up a perception of the environment in a similar way to their biological counterparts. Yet many radar systems bear only a passing resemblance to the echolocators of the natural world. Previous radar work has considered biomimetic and cognitive approaches related to echoic flow [1, 2], high range resolution profiles [2], dynamic parameter control [3], and adaptive waveform design [4, 5] (for more biologically-inspired radar techniques and approaches see [6]).

The techniques presented are developments of previous work by the same authors [7, 8] and employ similar techniques to work carried out in the sonar domain [9]. The authors' previous work focuses on magnitude-based approaches and the main novel contribution of this paper is the use of signal phase in experiment and analysis to locate a target in angle.

The paper is laid out as follows: in Section 1 we introduce natural localisation using acoustic signals; Section 2 provides the theoretical principles that underpin the signal processing and results; Section 3 presents the experimental technique used to test both biologically-inspired localisation techniques and the results of these experiments; a discussion of the results is carried out in Section 4; and conclusions and avenues of future work are given in Section 5.

In the remainder of this section we introduce the key signal properties shared by many echolocating species and give a brief overview of the most common auditory cues used by humans to locate sound sources. In addition we also indicate how these properties may be realised in a radar system and how analogous quantities to the localisation cues may be used by a radar. In doing so we lay the groundwork for the biologically-inspired radar techniques presented in the following sections.

1.1 Acoustic Echolocation

A large number of natural echolocators, including humans, bats, and dolphins share several features across their echolocation calls, despite the very different environments in which they operate.

Many echolocating species use wide acoustic bandwidths for echolocation; human expert echolocators use clicks with frequency content ranging across 2-13 kHz [10], bats calls use the 15-120 kHz range [11, 12], and dolphins have shown calls from 29-42 kHz[13]. It is worth noting that these signals have a large fractional bandwidth (bandwidth divided by centre frequency) of 1.47, 1.56, and 0.36 respectively. When considering wideband signals in the radar domain a similar fractional bandwidth may be achieved with a 2-6 GHz band (fractional bandwidth of 1). Further, because of the different speeds of acoustic and electromagnetic propagation, a radar signal at 3 GHz has approximately the same wavelength as a 3 kHz audio signal, and so we may expect some correspondence with echolocation in the scales of objects and environments that may be observed using a radar with comparable wavelengths.

There is evidence to suggest that several echolocators use very wide beamwidths to completely illuminate the space in front of them. This is true for human echolocators who have beamwidths of 120^o [10] and is true for certain species of bats which show dynamic control of their echolocation beamwidths in the range of 40-120^o [14]. To achieve a wide area of illumination in a radar system, an antenna with a suitably large beamwidth should be used.

Perhaps the most straightforward commonality between echolocators is the use of a binaural hearing configuration. The use of two ears to perceive sound enables the use of comparative localisation cues described in the following section.

The final and least understood feature of all echolocator activity is the cognitive processing used to interpret the reflected signals in the brain. It is known that there are certain signal properties (such as frequency and time delay) that are extracted in the lower brain from the reflected signals, and that these properties can be preserved and passed to higher levels of cognitive processing [15, 16]. What is not known is precisely what properties of signals are used by echolocators in order to perceive their environments. This is a very interesting area of active research, but is not considered further in this paper.

1.2 Psychoacoustic Cues

In the field of psychoacoustics there are several well-described cues that are used by people when localising the source of a sound [17–24]. These cues are:

- the Inter-Aural Level Difference (ILD)
- the Inter-Aural Time Difference (ITD)
- the Binaural Timbre Difference (BTD)

These cues are the subject of much psychoacoustic research and so only a brief overview is given here. All of these cues rely on the binaural nature of hearing, the ILD represents the power difference of a signal between the two ears. The largest contributing factor to the ILD is the head-shadow effect caused by the bulk of the head significantly attenuating sound signals, as a result the ILD is most useful for localisation of high-frequency signals [17, 23, 24]. The ILD finds its closest radar analogue in amplitude-comparison monopulse, where the radar compares the magnitude of the received signal at two antennas in order to locate a target.

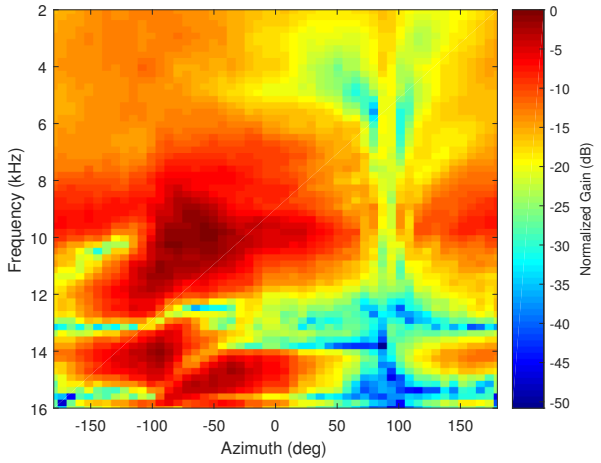

Fig. 1: Head-Related Transfer Function (HRTF) for a human left ear. Subject 003 from the CIPIC HRTF Database [26].

The ITD represents the Time Difference Of Arrival (TDOA) of a signal at the two ears. As a first-order estimate this may be considered to be the time difference caused by the geometrical path difference between the sound source and the two ears, but the reality is more complex and introduces frequency dependence to the cue, this results in the ITD being most significant for localisation of lower frequency sound sources [17, 18, 24, 25]. The closest radar analogue is TDOA.

The third cue, the BTD, can be thought of as how the timbre of a sound varies between the two ears. Timbre is the quality of a sound, and is composed of a complex layering of different tones and overtones, all with different magnitudes. Changes in timbre occur based on the direction of arrival of an acoustic signal because the mass of the head and the shape of the pinna (the outer ear) introduce direction-dependent filtering of acoustic signals. This filtering process can be described by the Head-Related Transfer Function (HRTF), an example from the CIPIC HRTF database [26] is shown in Figure 1. This HRTF shows how the power of a particular frequency component of an audio signal is attenuated by a human head and pinna which leads to an altered perception of the timbre of the sound [17, 19, 20, 22]. For instance, at an azimuth angle of 90^o, corresponding to the right of the person's head, the attenuation of a sound is at its highest due to the entire mass of the head being between this sound source and the left ear. There is no well-established radar analogue to the BTD and the HRTF, but it has been shown that a horn antenna exhibits frequency-dependent filtering of a radar signal and that this may be exploited for target localisation [7].

These cues may be exploited in the radar domain provided that there is a bistatic receiver configuration to enable comparison of the signals received at the two antennas.

2 Theory

2.1 Geometric Model

Figure 2 shows schematically the relative locations of the target; transmitter, Tx, with phase centre located at the origin; and pair of receivers, R_1 and R_2, located such that all three antennas are collinear. The receiving antennas are separated by a baseline, d. For a target located at a point, U, the time taken for a signal to reach each antenna can be expressed as in Equation 1, where c is the speed of light in a vacuum and the subscript i can take a value of either 1 or 2 to denote the relevant receiving antenna.

$$t_i = \frac{r_i + r_{\mathrm{tx}}}{c} \tag{1}$$

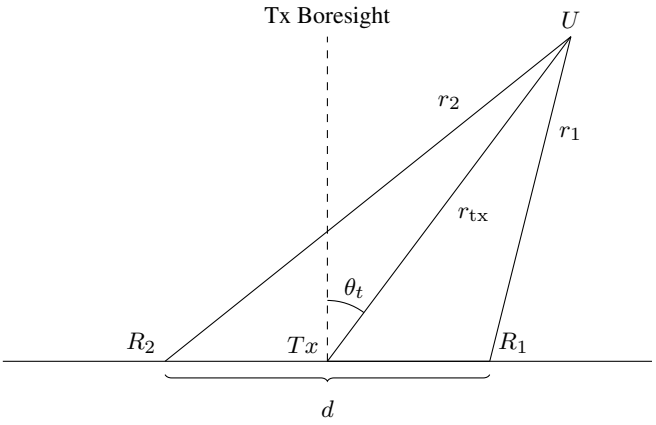

Fig. 2: System geometry for two receivers and a single transmitter in a binaural configuration.

2.2 Signal Description

The transmitted signal is given in Equation 2. This equation represents a linearly up-chirped signal of duration T.

$$s_{tx} \propto \exp\left(j\pi K t^2\right) \exp\left(j2\pi f_c t\right) \Pi\left(t, T\right) \tag{2}$$

Where f_c is the up-chirp starting frequency, K is the chirp rate (Hz/s), and $\Pi\left(t, T\right)$ is a boxcar function defined in Equation 3.

$$\Pi(t, T) = \begin{cases} 1 & \text{if } 0 \leq t \leq T \\ 0 & \text{otherwise.} \end{cases} \tag{3}$$

Recalling Equation 1 for the round-trip time taken by the signal allows us write Equation 4 for the received signal, which incorporates a time delay and a phase shift into the signal.

$$\begin{aligned} s_i^2 =& P_{Ri} \exp\left(j\pi K (t - t_i)^2\right) \exp\left(j2\pi f_c (t - t_i)\right) \\ & \Pi\left(t - t_i, T\right) \end{aligned} \tag{4}$$

2.3 Power Signal Ratio Approach

By taking inspiration from the ILD and the BTD, we can formulate a power-based angular localisation technique [7]. Beginning with the signal description from the previous section the radar equation for the power at the output of the receiving antenna is formulated as in Equation 5, with the relevent parameters described in Table 1.

$$P_{Ri} = \frac{P_{Tx} G_{Tx}(\theta_{\mathrm{t}}, \boldsymbol{f}) G_{Ri}(\theta_{\mathrm{t}} \pm \theta_0, \boldsymbol{f}) c^2 \sigma(\theta_{\mathrm{t}}, \boldsymbol{f})}{(4\pi)^3 \left(r_{tx} + r_i\right)^4 f^2 L(\theta_{\mathrm{t}})} \tag{5}$$

For a single measurement, there are several parameters that vary with frequency (including the target RCS and the attenuation in space), but providing that the antenna baseline d is sufficiently small $d << r_{tx}$, then the difference in these terms between the two receiving antennas is sufficiently small and is negligible. Considering the ratio of received signal powers between R_1 and R_2 yields Equation 6 and the interesting result that the signal ratio is independent of target range or reflectivity.

$$\begin{aligned} \frac{|s_1|^2}{|s_2|^2} =& \frac{\boldsymbol{P}_{R1}\left(\theta_{\mathrm{t}} + \theta_0, \boldsymbol{f}\right)}{\boldsymbol{P}_{R2}\left(\theta_{\mathrm{t}} - \theta_0, \boldsymbol{f}\right)} = \frac{\boldsymbol{G_{R1}}\left(\theta_{\mathrm{t}} + \theta_0, \boldsymbol{f}\right)}{\boldsymbol{G_{R2}}\left(\theta_{\mathrm{t}} - \theta_0, \boldsymbol{f}\right)} \\ =& \boldsymbol{A}\left(\theta_{\mathrm{t}}, \boldsymbol{f}\right) \end{aligned} \tag{6}$$

This result means that, by having prior information about the ratio of receiver gains across all angles of interest and all frequencies in

Table 1 Reference for mathematical symbols.

Symbol	Definition	Units
θ_{t}	target angle from transmitter boresight	radians
θ_0	receiver angle from transmitter boresight	radians
f	frequency	Hertz
P_{Ri}	signal power received at the i^{th} receiving antenna	Watts
P_{Tx}	power transmitted to the transmitting antenna	Watts
G_{Tx}	gain of the transmitting antenna	-
G_{Ri}	gain of the receiving antenna	-
c	speed of light in a vacuum	$\mathrm{m\ s^{-1}}$
σ	radar cross section (RCS) of the target	$\mathrm{m^2}$
L	losses	-

The subscript i is used throughout and can take a value of either 1 or 2 to denote the relevant receiving antenna.

the band, it is possible to build up a map function which describes the expected result of a measurement in the presence of a target. This map function depends only on the angle to the target and a known system characteristic (the antenna patterns), and is given in Equation 7, where $\boldsymbol{\theta}$ represents a set of all possible angles to a target.

$$\frac{\boldsymbol{G_{R1}}\left(\boldsymbol{\theta}+\theta_0,\boldsymbol{f}\right)}{\boldsymbol{G_{R2}}\left(\boldsymbol{\theta}-\theta_0,\boldsymbol{f}\right)}=\boldsymbol{M}\left(\boldsymbol{\theta},\boldsymbol{f}\right) \tag{7}$$

In this approach the signal ratio is the cue (and as with its acoustic counterpart requires some rudimentary processing in the processing chain) and the map function represents the prior information held by the system (analogous to the memory). What is required then, after a measurement is made, is some way of relating the measured signal ratio to the prior information held by the system. To do this, the Pearson correlation coefficient is calculated between the signal ratio and the frequency profile across each angle in the map function as formulated in Equation 8. Where $\sigma_{\boldsymbol{A}}$ and $\sigma_{\boldsymbol{M}}$ are the standard deviations of the signal ratio, $\boldsymbol{A}\left(\theta_{\mathrm{t}},\boldsymbol{f}\right)$, and the map function, $\boldsymbol{M}\left(\boldsymbol{\theta},\boldsymbol{f}\right)$, respectively. θ' represents a single angle from the set $\boldsymbol{\theta}$.

$$\boldsymbol{\rho}_A\left(\theta_t,\theta'\right)=\frac{\mathrm{cov}\left(\boldsymbol{A}\left(\theta_{\mathrm{t}},\boldsymbol{f}\right),\boldsymbol{M}\left(\theta',\boldsymbol{f}\right)\right)}{\sigma_{\boldsymbol{A}}\sigma_{\boldsymbol{M}}} \tag{8}$$

The Pearson correlation coefficients then represent the degree of similarity between the measured signal ratio and the expected profile at each candidate angle. By extracting the peak from this likelihood profile, the best estimate of the angle to the target is found.

2.4 Phase Difference Approach

This technique uses the same algorithmic structure as the power-based approach presented in Section 2.3, but instead relies on the phase of the received signals. There is much discussion in psychoacoustics about the extent with which humans and animals use phase differences to locate sound sources. However, for radar systems phase is fundamental and may therefore be used as the basis for a radar-only cue. A phase-only form of the radar equation is shown in Equation 9, and includes.

$$\begin{aligned}\boldsymbol{\phi}_{Ri}=\boldsymbol{\phi}_{Tx}+\angle\boldsymbol{G_{Tx}}(\theta_{\mathrm{t}},\boldsymbol{f})+\angle\boldsymbol{G_{Ri}}(\theta_{\mathrm{t}}\pm\theta_0,\boldsymbol{f})\\+\angle\sigma(\theta_{\mathrm{t}},\boldsymbol{f})+\frac{4\pi\left(r_{tx}+r_i\right)\boldsymbol{f}}{c}\end{aligned} \tag{9}$$

Conventionally antenna gain is written as a real quantity, however over the wide frequency band used by this technique the phase centre of each antenna varies. This phase centre variation modulates the received signal with a frequency- and angle-dependent phase-shift, which can be incorporated into the antenna gain terms by considering them as complex quantities (modifying both the amplitude and phase of the transmitted or received signal). The angles of the complex gains then represent the phase-shift that the antennas introduce.

The measured signal phase difference between the two receiving antennas is then evaluated in Equation 10, which shows that target-dependent phase effects cancel-out.

$$\begin{aligned}\boldsymbol{\Phi_S}\left(\theta_{\mathrm{t}},\boldsymbol{f}\right)=&\boldsymbol{\phi}_{R1}-\boldsymbol{\phi}_{R2}\\=&\angle\boldsymbol{G_{R1}}(\theta_{\mathrm{t}}+\theta_0,\boldsymbol{f})-\angle\boldsymbol{G_{R2}}(\theta_{\mathrm{t}}-\theta_0,\boldsymbol{f})\\&+\frac{4\pi r_1\boldsymbol{f}}{c}-\frac{4\pi r_2\boldsymbol{f}}{c}\end{aligned} \tag{10}$$

This formulation means that the measured signal is a function of prior information, the angle to the target, and the bistatic ranges to the target. However, the range dependence can be approximated as $d\sin(\theta)$ provided that the condition $d << r_{tx}$ is satisfied, this replaces the range dependence and hence a phase map function (purely a function of angle and frequency) can be formulated as in Equation 11. The phase map function gives the expected phase difference between the antennas for a target at a given angle and across all transmitted frequencies.

$$\begin{aligned}\boldsymbol{\Phi_M}\left(\boldsymbol{\theta},\boldsymbol{f}\right)=&\angle\boldsymbol{G_{R1}}(\theta_{\mathrm{t}}+\theta_0,\boldsymbol{f})-\angle\boldsymbol{G_{R2}}(\theta_{\mathrm{t}}-\theta_0,\boldsymbol{f})\\&+\frac{2\pi d\boldsymbol{f}}{c}\sin\left(\theta_{\mathrm{t}}\right)\end{aligned} \tag{11}$$

$$\boldsymbol{\rho_S}\left(\theta_t,\theta'\right)=\frac{\mathrm{cov}\left(\boldsymbol{\Phi_S}\left(\theta_{\mathrm{t}},\boldsymbol{f}\right),\boldsymbol{\Phi_M}\left(\theta',\boldsymbol{f}\right)\right)}{\sigma_{\boldsymbol{\Phi_S}}\sigma_{\boldsymbol{\Phi_M}}} \tag{12}$$

In this approach, the signal phase difference is the utilised cue and the phase map function contains the prior information about the system characteristics. It is then possible to compare the measured signal phase difference with each frequency profile in the phase map function using the Pearson correlation coefficient. The Pearson correlation coefficient is given in Equation 12, where $\sigma_{\boldsymbol{\Phi_S}}$ and $\sigma_{\boldsymbol{\Phi_M}}$ refer to the standard deviations of the measured signal phase difference, $\boldsymbol{\Phi_S}$, and the phase map function, $\boldsymbol{\Phi_M}$, respectively. The highest (closest to 1) value of the coefficient represents the angle at which the target is most likely to be located.

2.5 On-Boresight Detection

The techniques presented in the previous sections rely on the Pearson correlation coefficient to estimate the angle to the target. This method is deficient in the boresight direction because the Pearson correlation coefficient is independent of the powers of the functions being correlated. In the boresight direction, the difference between the measured signals (in both power and phase approaches) is zero across all frequencies, and so the effect of noise present on the signal is amplified in the correlation process. To compensate for this deficiency, a technique is introduced whereby the system identifies that it has a target in the region of poor performance, and switches to a traditional monopulse approach (which performs well in the boresight direction) for angular localisation.

To identify if the system is in the region of poorest performance, a measure of angular variance may be used as the signal difference is always approximately zero in the boresight direction. The angular variance metric is the standard deviation of the measured frequency profile, given in Equation 13 where $\boldsymbol{S}\left(\theta_{\mathrm{t}},\boldsymbol{f}\right)$ is understood to be either the power-based signal ratio, $\boldsymbol{A}\left(\theta_{\mathrm{t}},\boldsymbol{f}\right)$, or the phase difference, $\Phi_S\left(\theta_{\mathrm{t}},\boldsymbol{f}\right)$, depending on the technique being used. $\bar{S}$ is the mean value of $\boldsymbol{S}$ across all measured frequencies, N_f is the number of frequency components in $\boldsymbol{S}$, and f_i is the i^{th} component of the frequency vector $\boldsymbol{f}$.

$$\boldsymbol{\sigma_S}=\sqrt{\frac{\sum_{i=1}^{N_f}\left(S\left(\theta_{\mathrm{t}},f_i\right)-\bar{S}\right)^2}{N_f}} \tag{13}$$

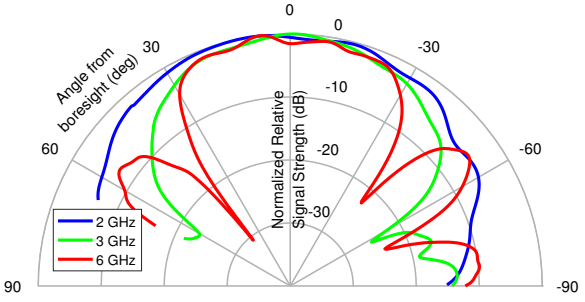

Fig. 3: Antenna pattern measured across a 2-6 GHz band, showing 3dB beamwidths of approximately 120^o at 2 GHz and 60^o at 6 GHz.

If this metric falls below a pre-defined threshold, a traditional phase-comparison monopulse technique is used. The phase-comparison monopulse technique used [27] is shown in Equation 14, where f_m is the single frequency chosen for monopulse.

$$\theta_{\mathrm{t}} = \arcsin\left(\frac{c\Phi_S\left(f_m\right)}{2\pi d\boldsymbol{f}}\right) \tag{14}$$

3 Experiment

3.1 Measuring Method

Horn antennas from Q-par Angus (WBH1-18) which satisfied the requirements of a wide beamwidth and a wide operational bandwidth were used; Figure 3 shows how the antenna beamwidth varies across the 2-6 GHz frequency band, presenting a broad beam with beamwidths of approximately 120^o at 2 GHz and 60^o at 6 GHz. In order to mimic the binaural hearing configuration of echolocators two spatially-separated identical receiving antennas were used, as presented in Section 2.1. Because of the use of a 'binaural' receiver configuration, the cues discussed in Section 1.2 may be utilised by the radar system. To complete the biological analogy a third identical antenna was used exclusively for the transmit signal, mimicking the central placement of the mouth, the origin of echolocator clicks. The transmit antenna pattern was not a factor in the signal processing due to its absence in Equations 6 and 10, but it did affect the SNR of the received signals.

The antennas were mounted in a configuration broadly mimicking nature, as shown in Figure 4, and were placed with a target in an anechoic chamber. Due to the limited space available in the chamber, the target could not be moved through the required range of azimuth angles. Instead the antennas were mounted on a rotation table such that, relative to the transmit antenna boresight direction, measurements could be made over the desired range of angles to the target. The target, a single mirrored sphere of 36cm diameter, was placed on a plinth to raise it into the same plane as the antennas, at a distance of approximately 3m.

The physical size of the antennas places a lower limit on their separation. When this restriction is combined with the maximum target range in the anechoic chamber (approximately 3m), the assumption that $d << r_{tx}$ is no longer valid and introduces an error term to Equation 11. To mitigate this, the antenna calibration is performed from this range, which cancels out the error. For this technique to be viable at short ranges the antenna separation should be minimal, as the target range increases the geometric errors are expected to reduce.

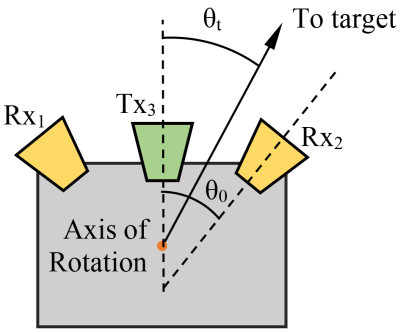

Fig. 4: The biologically-inspired radar configuration.

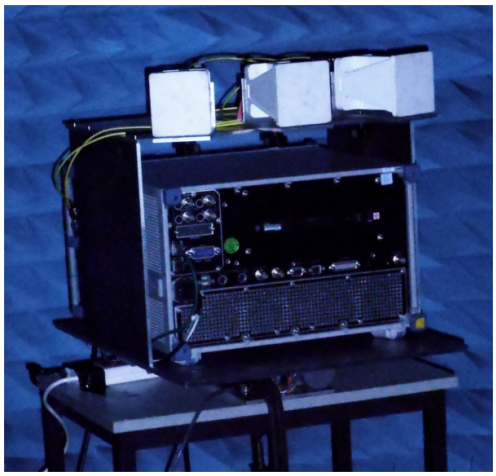

Fig. 5: The experimental setup using the vector network analyzer (ZVA-67) and three wideband horn antennas.

A vector network analyser (VNA) was used to generate the require band of frequencies. The VNA was placed on the rotation table below the antennas as shown in Figure 5 to maintain phase coherence (by avoiding flexing of cables). The VNA used was a 4-port Rohde & Schwarz ZVA-67 which has a very low noise floor (at approximately -120 dBm). The rotation table used was a Parker 200RT which has a positioning accuracy of approximately 0.03^o and was therefore suitable to make measurements at 0.5^o intervals across a range of -90^o to $+90^o$ to the target.

The measurements made consisted of s_1 and s_2 measured across a frequency band of 2-6 GHz with a frequency step of 10 MHz. In order to minimise the clutter response of the chamber, an initial background measurement of the environment (across -90^o to $+90^o$ and across the 2-6 GHz band) was made in the absence of the target, and was subtracted from all subsequent measurements made in the presence of a target.

3.2 Signal Processing

The signals, s_1 and s_2, were measured in the frequency domain, and were transformed into the time domain using the Fast Fourier Transform (FFT). In the time domain, direct-path signals (signals received without reflection directly from the transmitter) and reflections from the experimental apparatus corrupt the signal. A range-azimuth map in the presence of the target can be seen in Figure 6a which shows the effect of clutter in the environment. In this range-azimuth map, the target is visible to -20 dB over an angular region of approximately 100^o which is in agreement with the antenna pattern presented in Figure 3. A range-azimuth map of the chamber without a target is shown in Figure 6b. This figure shows that the direct signal and low-range clutter dominate the returns. The target was then windowed within 25 range bins (0.935 m) in order to reduce the effects of this clutter. The windowed region was extracted and zero-padded before

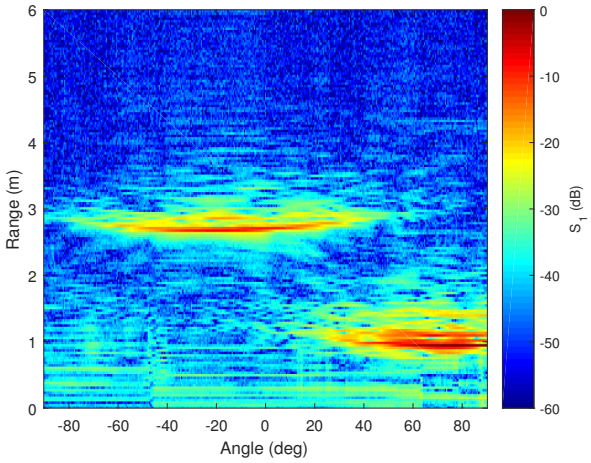

(a) The chamber with the target. Here, clutter is visible at low angles. The clutter at a range of 1m at 20^o-90^o is caused by a pillar that was placed in the corner of the chamber behind the apparatus.

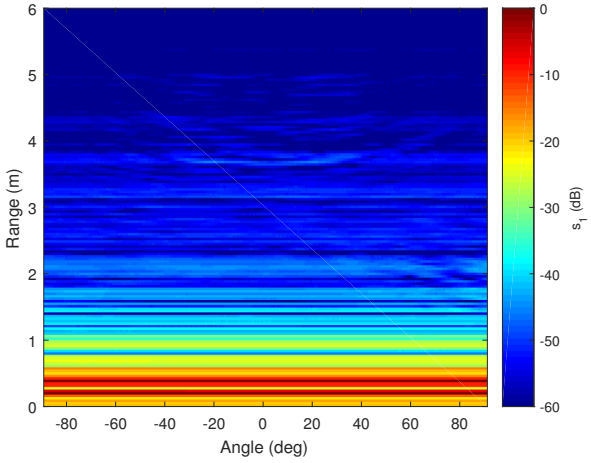

(b) The chamber without the target. The direct signal can be seen to dominate the returns at low ranges.

Fig. 6: Range-azimuth maps of the anechoic chamber.

transforming back into the frequency domain through the use of an Inverse Fast Fourier Transform.

The measurements of the antenna patterns were made by placing an antenna on the plinth at the far end of the chamber, pointed directly at the receiving antennas. As a result of this configuration, the directly received signal dominates the return and clutter is not significant. Before correlating with the measured signal profile, the map function was down-sampled to match the dimensions of the up-sampled measured signal.

3.3 Biologically-Inspired Antenna Cue Results

For the power-based approach, the powers $|s_1|^2$ and $|s_2|^2$ are calculated before dividing the signals which results in the measured signal ratio (evaluated over several measurements at different angles) shown in Figure 8a. By the same method, the power map function is evaluated and is shown in Figure 8b. In the phase-based approach, the phases $\angle s_1$ and $\angle s_2$ are calculated before subtracting the signals which results in the measured signal phase difference(evaluated over several measurements at different angles) shown in Figure 9a. As described in Section 2.4, the phase map function is evaluated and is shown in Figure 9b.

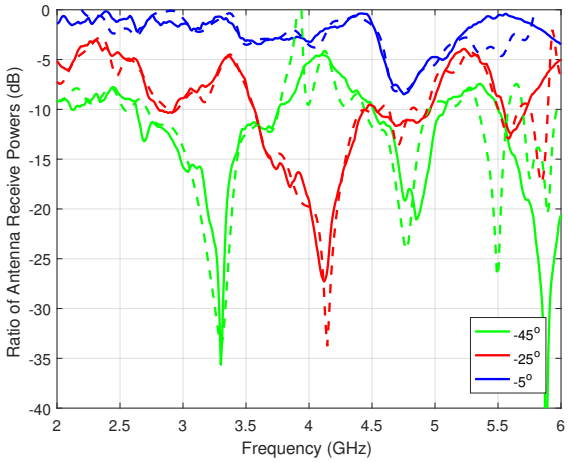

Fig. 7: Three sample frequency profiles taken from the signal ratio and the map function (Figures 8a and 8b respectively). Solid lines show the measurements predicted by the map function and dashed lines show the signal ratios from measurements made in the presence of a target.

Here, the map functions indicate a coding of space as a function of frequency by the antennas and show the expected result of measurements in the presence of a target at any possible angle. For example, Figure 7 shows three sample frequency profiles from the map function, each of which is unique to that angle. When compared to the corresponding sample profiles from the signal ratio there is a high correlation. More generally it can be seen that there is good agreement between the spectral structures present in the signal ratio and those present in the map function. The most significant disagreement occurs further from the boresight direction where noise corrupts the signal and the signal-to-noise ratio (SNR) decreases. Once the map functions have been measured for a particular configuration of antennas, the system can be moved to any environment, providing that the relative positions and orientations of the antennas remain fixed.

The correlation was then computed using the Pearson correlation coefficient as described in Equation 8 and shown in Figures 8c and 9c, and the peaks were extracted and used to estimate the angular location of the target for each measurement. The error between the estimated angle and the correct angle to the target was then plotted and can be seen in Figures 8d and 9d for power- and phase-based approaches respectively.

The power-based method is capable of localising the target in azimuth with an error of 2.48^o over the range $0^o \leq \theta \leq 70^o$, and the phase-based approach locates the target in azimuth with an error of 1.80^o over the range $0^o \leq \theta \leq 70^o$.

3.4 On-Boresight Detection Results

The technique described in Section 2.5, in which the system determines if it is on or near boresight, was applied to the experimental data used in the previous sections. The monotone frequency used for phase-comparison monopulse was 2.03 GHz. Different selection criteria were applied to the two methods, a threshold of 3.75 dB was used for the power approach as shown in Figure 10a, while for the phase approach a threshold of 1 radian was used and can be seen in Figure 10b. Using these thresholds the results in Figures 10c-10d show that meaningful improvement in angular localisation performance can be achieved. For the power-based signal ratio approach the angular location error was reduced to 1.75^o over the range $0^o \leq \theta \leq 70^o$, while the phase comparison approach had an error now down to 0.84^o over the range $0^o \leq \theta \leq 70^o$.

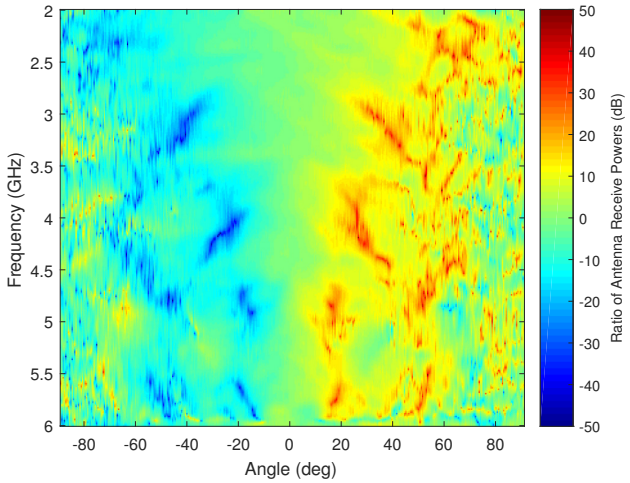

(a) Signal ratio measured in the presence of target.

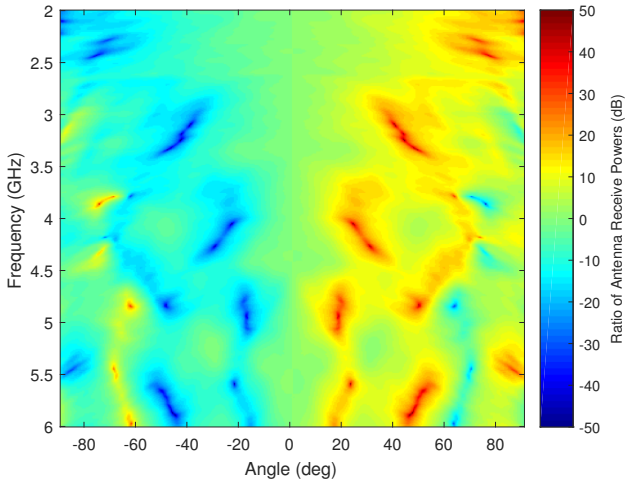

(b) Power map function.

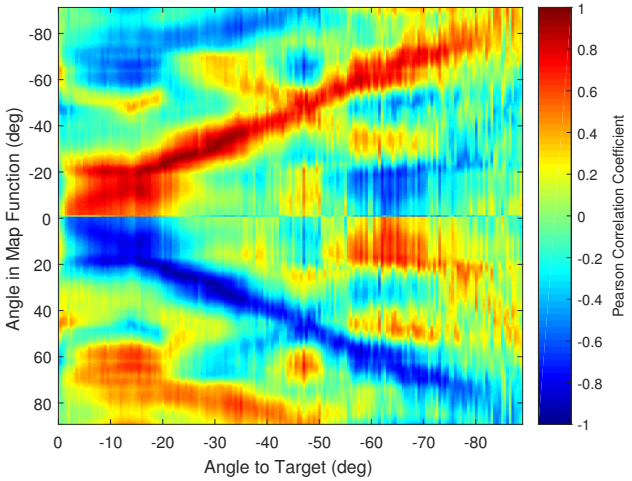

(c) Result of the Pearson correlation between each frequency profile in the map function and the signal ratio, using the power-based approach.

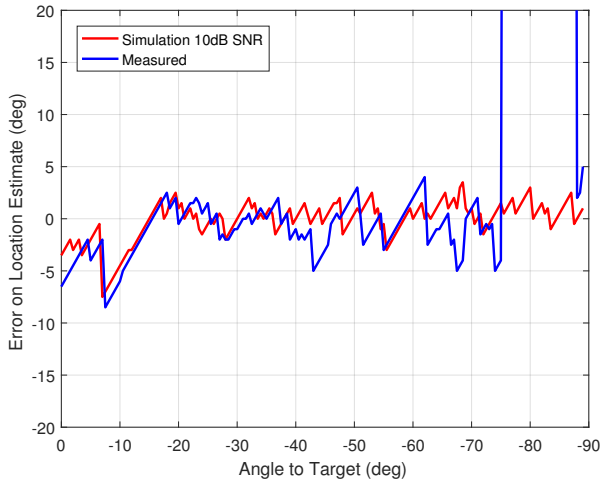

(d) Result for target localisation in azimuth using the power-based HRTF technique. Simulation results for 10dB SNR are shown in red, and measurement results (with variable SNR) are in blue.

Fig. 8: Results for the power-based approach

4 Discussion

4.1 Single Target and Full-Bandwidth

The results presented in the previous section show that the biologically-inspired radar cues allow for good angular localisation performance over a wide angle of operation. A 'rule of thumb' for monopulse techniques is that target angular location accuracy can be performed to approximately 10% of the antenna beamwidth. For example, the narrowest beam present in the used band (at 6 GHz) has a beamwidth of approximately 60^o, and so the rule of thumb would indicate that the angular location accuracy should be only 6^o subject to an SNR of approximately 15 dB. Both techniques outperform this figure, and have a wider range of operation. This descriptive result demonstrates that these biologically-inspired techniques can extend the performance and range of existing radar methodologies.

It is worth noting that in Figure 8d the measured result underperforms the simulation result. The simulation was conducted at a fixed SNR, but the measurement is subject to real-world SNR variations causing the SNR to drop at angles away from the boresight direction, as shown in Figure 11. The measurements of SNR on the signals s_1 and s_2 are used to estimate the SNR on the joint pattern using Equation 15 [7]. From this estimate of the SNR on the joint pattern it can be seen that the SNR drops to below 10dB at approximately -60^o, consistent with the measured performance suffering for angles further from the boresight.

$$\mathrm{SNR}_{\mathrm{joint}} = \left(\mathrm{SNR}_1{}^{-2} + \mathrm{SNR}_2{}^{-2}\right)^{-0.5} \tag{15}$$

In both the phase difference approach and the power signal ratio approach, the performance is worst in the boresight direction, despite the SNR being at its largest in this direction. This effect is due to the absence of difference between both techniques at 0^o across all frequencies of the band. As the Pearson correlation coefficient does not depend on signal magnitude, even a small quantity of noise correlates more highly with an angular profile with any deviation from zero. To compensate for this effect the boresight identification technique was used for both methods to select when to use the biologically-inspired techniques, and when to use traditional monopulse techniques. The results shown in Section 3.4 indicate that it is possible to significantly improve performance of the techniques in the boresight direction using this technique, resulting in the errors on techniques shown in Table 2.

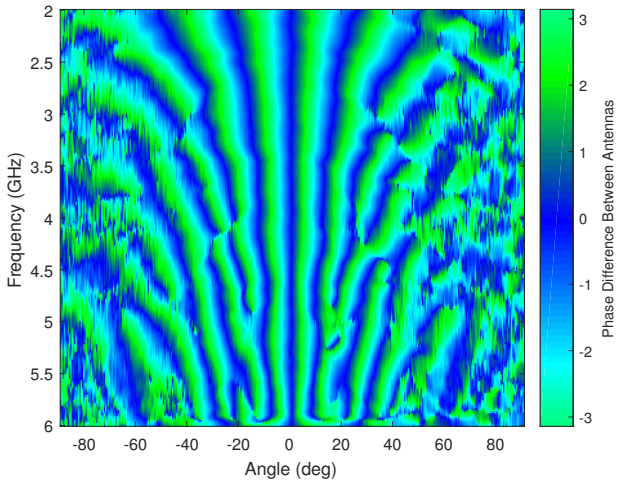

(a) Signal phase difference measured in the presence of target.

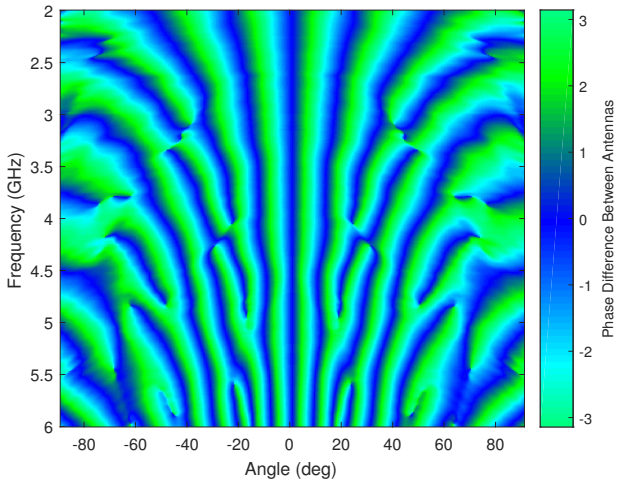

(b) Phase map function.

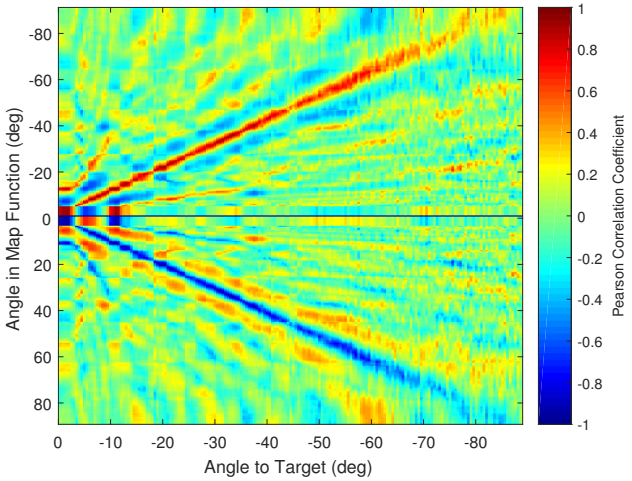

(c) Result of the Pearson correlation between each frequency profile in the map function and the signal phase difference using the phase-based approach.

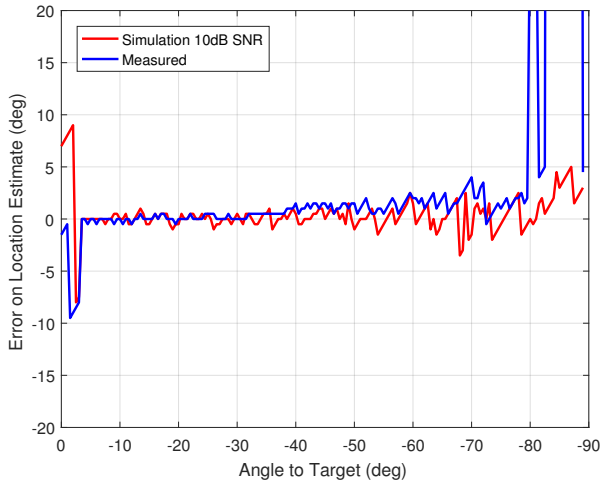

(d) Result for target localisation in azimuth using the phase-based HRTF technique. Simulation results for 10dB SNR are shown in red, and measurement results (with variable SNR) are in blue.

Fig. 9: Results for the phase-based approach

Table 2 Angular location error in degrees on biologically-inspired methods for different angular regions, with and without on-boresight detection and correction using a traditional phase monopulse approach.

	Power Signal Ratio		Phase Difference	
On-Boresight Detection	Without	With	Without	With
0-70^o	2.48	1.75	1.80	0.84
0-40^o	2.68	1.30	1.99	0.36
20-40^o	1.14	1.14	0.36	0.36

4.2 Performance effects of different frequency bands

To examine the performance of both power- and phase-based approaches with different frequency bands, a subset of the collected data was processed independently to emulate measurements with a 2-4 GHz band and a 2-5 GHz band. The results for the power- and phase-based approaches are shown in Figure 12. From these figures it can be seen that the overall performance suffers for each technique as the bandwidth is decreased. This degradation of performance is more severe for the power-based approach than the phase-based approach, and affects the angular regions near the boresight direction (0^o) and near 90^o most significantly, leaving the region surrounding 45^o with the most stable performance in all cases.

5 Conclusion

In this paper we have shown that it is possible to take inspiration from the biological worlds of echolocation and sound localisation in order to present a wideband radar technique that is capable of high accuracy angular localisation over a wide range of azimuth angles. By using a wide bandwidth we have also explored ways to exploit the natural coding introduced by antennas over a wide bandwidth and have shown that it is possible to use this to enable angular target localisation.

We have also shown that by combining a traditional phase-comparison monopulse technique with the novel wideband angular localisation techniques presented, performance superior to either isolated technique may be achieved.

Future work developing these techniques to integrate the power- and the phase-based approaches should improve the performance

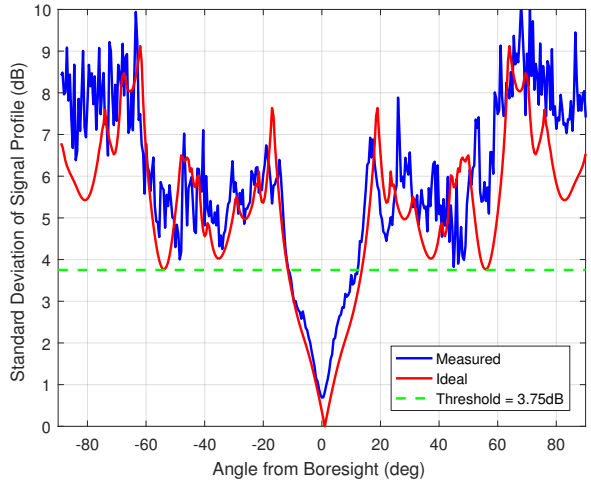

(a) Angular variance, power approach.

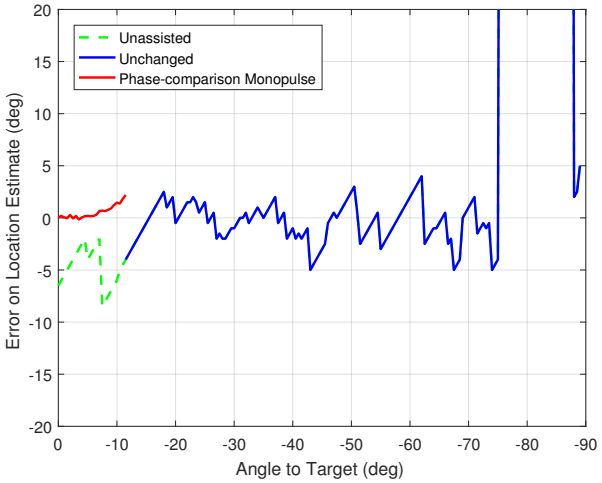

(c) Accuracy results, power approach.

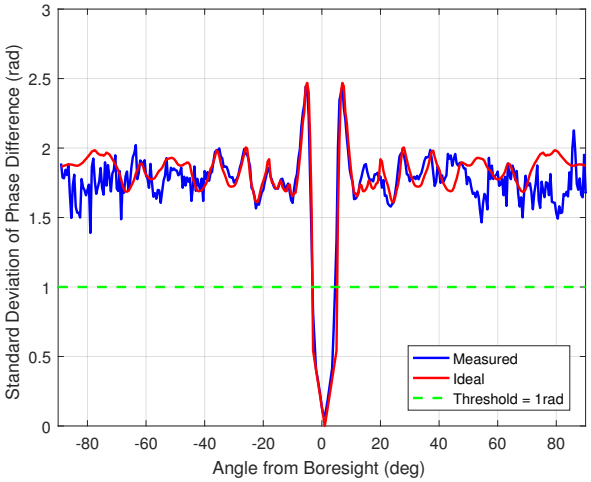

(b) Angular variance, phase approach.

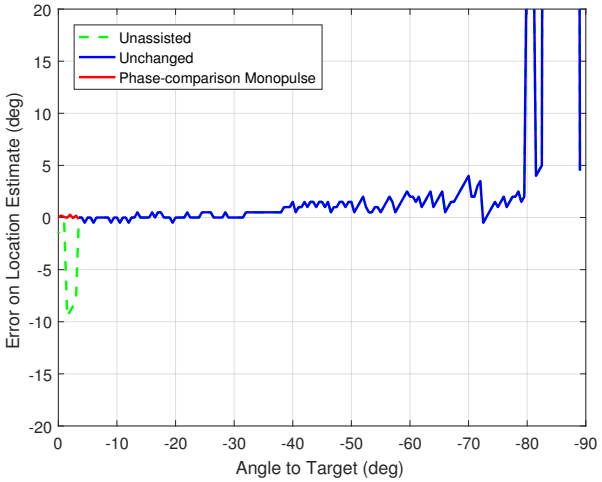

(d) Accuracy results, phase approach.

Fig. 10: Results with the boresight identification and correction algorithm

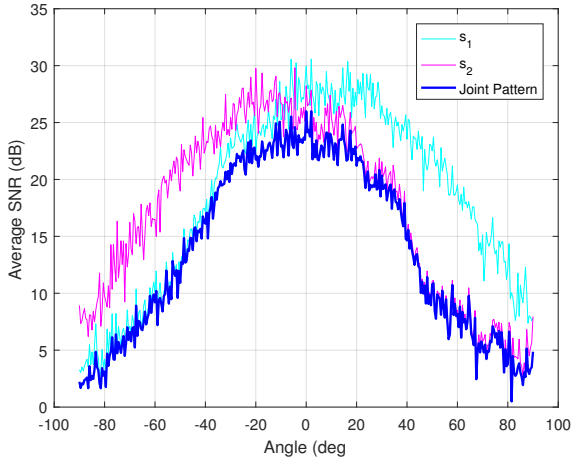

Fig. 11: SNR on each of the received signals, and the SNR estimated on the joint pattern.

and robustness of angular localisation. The issues introduced by closely-spaced targets merit more research as solving these would allow more complex environments such as those with significant multipath to be investigated. Field trials would enable the $d << r_{tx}$ condition to be convincingly satisfied and could provide useful insight into how this technique could be implemented in practice. Optimisation of the antenna patterns could provide a way to reduce the bandwidth of the technique and improve performance.

6 Acknowledgments

The authors thank the EPSRC for their support of this work.

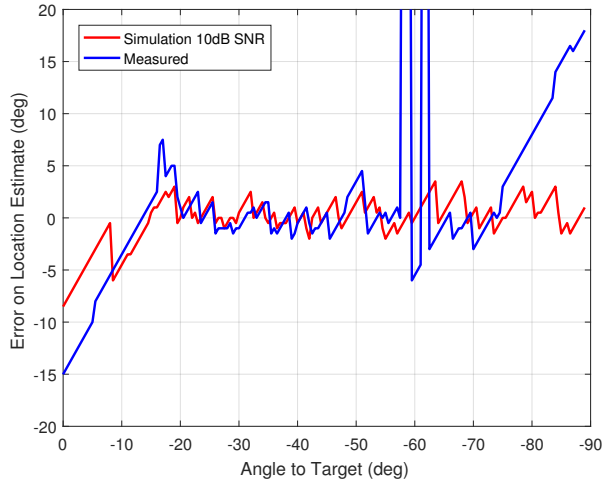

(a) 2-5 GHz, Power-based approach

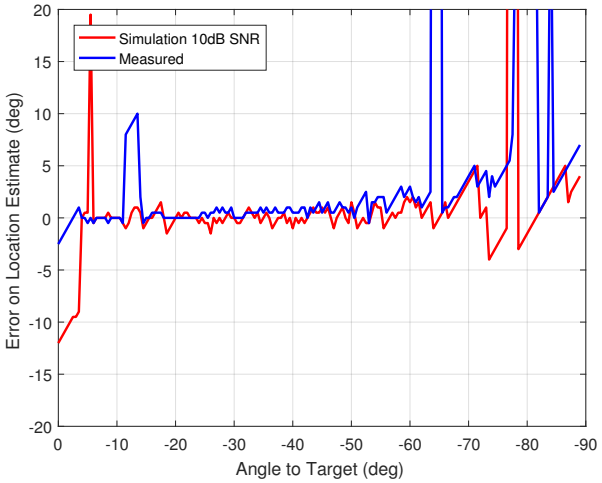

(c) 2-5 GHz, Phase-based approach

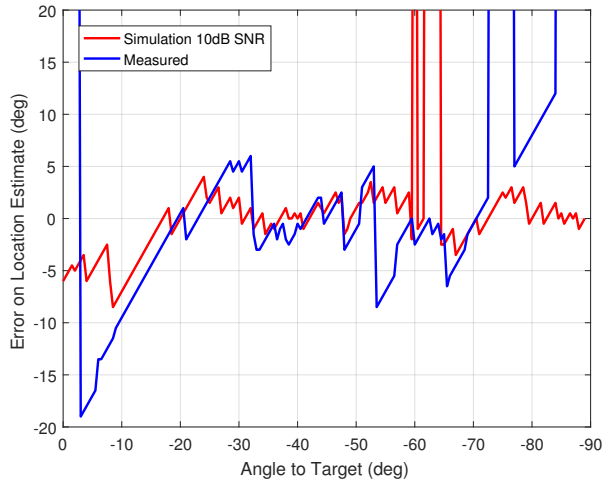

(b) 2-4 GHz, Power-based approach

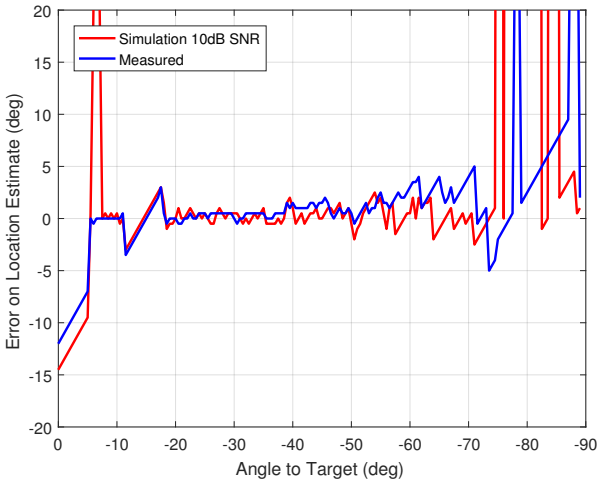

(d) 2-4 GHz, Phase-based approach

Fig. 12: Result for target localisation in azimuth using the phase-based HRTF technique for different sub-bands. Simulation results for 10dB SNR are shown in red, and measurement results (with variable SNR) are in blue.

7 References

1 Smith, G.E., Baker, C.J., Li, G. 'Coupled echoic flow for cognitive radar sensing'. In: 2013 IEEE Radar Conference (RADAR). (Ottawa, 2013). pp. 1–6

2 Baker, C.J., Smith, G.E., Balleri, A., et al.: 'Biomimetic Echolocation With Application to Radar and Sonar Sensing', *Proceedings of the IEEE*, 2014, **102**, (4), pp.447–458

3 Vespe, M., Jones, G., Baker, C.J.: 'Lessons for Radar', *IEEE Signal Processing Magazine*, 2009, **26**, (1), pp.65–75

4 Goodman, N.A., Venkata, P.R., Neifeld, M.A.: 'Adaptive Waveform Design and Sequential Hypothesis Testing for Target Recognition With Active Sensors', *IEEE Journal of Selected Topics in Signal Processing*, 2007, **1**, (1), pp.105–113

5 Guerci, J.R. 'Cognitive radar: A knowledge-aided fully adaptive approach'. In: 2010 IEEE Radar Conference. (Arlington, 2010). pp. 1365–1370

6 Balleri, A., Griffiths, H., Baker, C.: 'Biologically-Inspired Radar and Sonar: Lessons from Nature'. (Institution of Engineering and Technology, 2017

7 Reich, G.M., Antoniou, M., Baker, C.J. 'Frequency-dependent target localization'. In: IET International Conference on Radar Systems (Radar 2017). (Belfast, 2017).

8 Reich, G.M., Antoniou, M., Baker, C.J. 'Bio-Inspired Techniques for Target Localization'. In: 2018 IEEE Radar Conference. (Oklahoma City, 2018).

9 Reijniers, J., Peremans, H.: 'Biomimetic Sonar System Performing Spectrum-Based Localization', *IEEE Transactions on Robotics*, 2007, **23**, (6), pp.1151–1159

10 Thaler, L., Reich, G., Zhang, X., et al.: 'Mouth-clicks used by blind expert human echolocators - signal description and model based signal synthesis', *PLoS Computational Biology*, 2017, **13**, (8)

11 Siemers, B.M., Schnitzler, H.U.: 'Natterer's bat (Myotis nattereri Kuhl, 1818) hawks for prey close to vegetation using echolocation signals of very broad bandwidth', *Behav Ecol Sociobiol*, 2000, **47**, (6), pp.400–412

12 Foote, K.G., Simmons, J.A.: 'Bat sonar and the role of frequency diversity', *The Journal of the Acoustical Society of America*, 2006, **119**, (5), pp.3318–3318

13 Ibsen, S.D., Au, W.W.L., Nachtigall, P.E., et al.: 'Functional bandwidth of an echolocating Atlantic bottlenose dolphin (Tursiops truncatus)', *J Acoust Soc Am*, 2009, **125**, (2), pp.1214–1221

14 Jakobsen, L., Olsen, M.N., Surlykke, A.: 'Dynamics of the echolocation beam during prey pursuit in aerial hawking bats', *Proc Natl Acad Sci U S A*, 2015, **112**, (26), pp.8118–8123

15 Kolarik, A.J., Cirstea, S., Pardhan, S., et al.: 'A summary of research investigating echolocation abilities of blind and sighted humans', *Hear Res*, 2014, **310**, pp.60–68

16 Noggle, C.A. 'Auditory Cortex'. In: Goldstein, S., Naglieri, J.A., editors. Encyclopedia of Child Behavior and Development. (Springer US, 2011). pp. 171–172

17 Woodworth, R.S. 'Hearing'. In: Experimental psychology / Robert S. Woodworth. (Methuen, 1950). pp. 501 – 538

18 Feddersen, W.E., Sandel, T.T., Teas, D.C., et al.: 'Localization of High-Frequency Tones', *The Journal of the Acoustical Society of America*, 1957, **29**, (9), pp.988–991

19 Freedman, S.J., Fisher, H.G. 'The role of the pinna in auditory localization'. In: Freedman, S.J., editor. The neuropsychology of spatially oriented behavior / edited by Sanford J. Freedman.. 1st ed. Dorsey series in psychology. (Homewood Illinois: Dorsey Press, 1968). pp. 135–152

20 Hebrank, J., Wright, D.: 'Spectral cues used in the localization of sound sources on the median plane', *The Journal of the Acoustical Society of America*, 1974, **56**, (6), pp.1829–1834

21 Middlebrooks, J.C., Green, D.M.: 'Sound Localization by Human Listeners', *Annual Review of Psychology*, 1991, **42**, (1), pp.135–159

22 Wightman, F.L., Kistler, D.J. 'Sound Localization'. In: Fay, R.R., Popper, A.N., Yost, W.A., editors. Human psychophysics / William A. Yost, Arthur N. Popper, Richard R. Fay, editors. Springer handbook of auditory research ; v. 3. (Springer-Verlag, 1993). pp. 155 – 192

23 Blauert, J. 'Evaluating Nonidentical Ear Input Signals'. In: Spatial hearing: the psychophysics of human sound localization. rev. ed ed. (Cambridge, Mass: MIT

Press, 1997). pp. 137–177
24 Shinn.Cunningham, B.G., Santarelli, S., Kopco, N.: 'Tori of confusion: Binaural localization cues for sources within reach of a listener', *The Journal of the Acoustical Society of America*, 2000, **107**, (3), pp.1627–1636
25 Kuhn, G.F.: 'Model for the interaural time differences in the azimuthal plane', *The Journal of the Acoustical Society of America*, 1977, **62**, (1), pp.157–167
26 Algazi, V.R., Duda, R.O., Thompson, D.M., et al. 'The CIPIC HRTF database'. In: Applications of Signal Processing to Audio and Acoustics, 2001 IEEE Workshop on the. (New York, 2001). pp. 99–102
27 Kingsley, S., Quegan, S. 'Tracking Radar'. In: Understanding Radar Systems. (SciTech Publishing, 1999). p. 52